Nanoscale

Accepted Manuscript

This article can be cited before page numbers have been issued, to do this please use: K. S. Suraj, J. Gutiérrez Moreno and M. H. N. Assadi, *Nanoscale*, 2026, DOI: 10.1039/D6NR00211K.

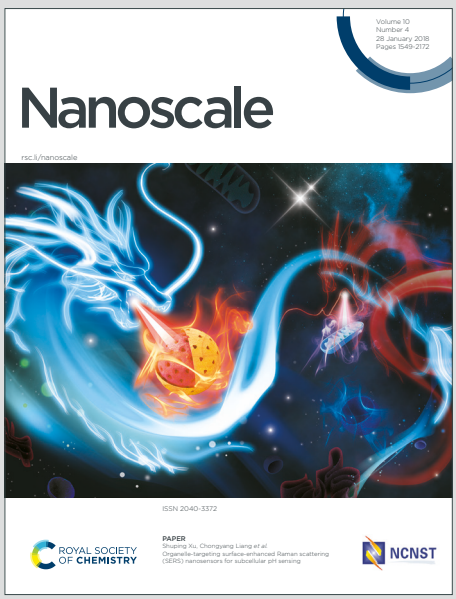

ROYAL SOCIETY OF CHEMISTRY

rsc.li/nanoscale

View Article Online
DOI: 10.1039/D6NR00211K

Journal Name

ARTICLE TYPE

Cite this: DOI: 00.0000/xxxxxxxxxx

$4f$ Band Modulation by Spin-Orbit Coupling in Low-Dimensional Rare Earth Catalysts†

Kabir S. Suraj,*[a] J. Julio Gutiérrez Moreno,[b] and M. Hussein N. Assadi*[a,c]

Received Date
Accepted Date

DOI: 00.0000/xxxxxxxxxx

We report a first-principles study of Eu nano-sheets of varying thickness supported on a rutile TiO_2 surface, focusing on the influence of spin-orbit coupling (SOC) and sheet thickness on the Eu $4f$ electronic structure and its catalytic implications. Using both collinear and non-collinear density functional theory with on-site Coulomb corrections (DFT+U) and van der Waals dispersion, we construct and relax interface models comprising single atoms, monolayers, bilayers, and quadruple layers of Eu. Layer-resolved density of states (DOS) analysis reveals that SOC lifts the degeneracy of the Eu $4f$ states, broadening their spectrum and shifting the principal DOS peaks closer to the Fermi-level. For example, in the single-atom Eu configuration, SOC shifts the maximum $4f$ DOS peak from -0.759 eV to -0.063 eV while increasing the spectral width from 0.133 eV to 0.680 eV. A clear correlation emerges between the Eu−O interfacial distance and the localisation of the $4f$ states, with thicker Eu nano-sheets exhibiting sharper and more deeply bound electronic states. These results suggest that ultra-thin Eu configurations with SOC-broadened $4f$ states may enhance electron transfer to adsorbed intermediates, making them promising candidates for catalytic processes such as water splitting, hydrogen evolution, and hydrocarbon reforming.

1 Introduction

Lanthanide catalysts exhibit unique chemical characteristics that enable highly selective and efficient transformations, establishing these elements as pivotal materials in advanced catalytic applications [1–3]. The lanthanide metals exhibit strong Lewis acidity and provide multiple accessible reaction pathways, rendering them valuable in various selective processes, including hydrogenation, hydrosilylation, hydroboration, enantioselective reactions [4], and dehydrogenation [5]. A notable feature of the lanthanide is their strong oxophilicity, facilitating the formation of stable bonds with oxygenated intermediates during water-splitting reactions [6]. Such interactions allow for rapid water adsorption, molecular dissociation, and stabilisation of reactive intermediates—key steps for achieving efficient oxygen and hydrogen evolution reactions [7].

More specifically, given the quest for low-emission energy sources, hydrogen stands out as a clean and versatile fuel, intensifying the search for efficient production catalysts. Through nano-engineering, lanthanide offer remarkable potential for hydrogen production due to their tunable structural and electronic properties in reactions such as steam methane reforming and auto-thermal reforming of hydrocarbons [8,9]. Furthermore, lanthanide metals exhibit exceptional durability under extreme industrial conditions such as high temperatures and pressures, ensuring long-term catalyst performance with minimal maintenance [10]. Their alloying capability further enhances catalytic activity; for instance, NdTe hollow-shell nano-alloys, formed by combining Nd and Te, show outstanding hydrogen production efficiency via alkaline water electrolysis [11].

In practice, metal catalysts are formed by synthesising metallic nano-particles on a nano-porous support. This support can be either an oxide (silica, Titania, ceria, etc.) [12], a carbon nano-structure (graphene [13] or C nano-tubes [14] and nano-flakes [15]), or a metal-organic framework [16]. However, the electronic interactions between the metallic nano-particles and the supporting material through orbital hybridisation are often overlooked [17]. This hybridisation may be minimal for larger metallic nano-particles with dimensions above ≈ 10 nm or of specific shapes, as only a small percentage of the metallic atoms are in direct contact with the support. However, hybridisation becomes significant for smaller sizes and morphologies, such as nano-flakes, as a greater portion of the metallic nano-alloy interacts with the support. As a result, the observed catalytic performance may be equally influenced by the orbital rearrangements in the metallic nano-particles caused by electronic hybridisation with the supporting substrate.

Recent studies have demonstrated that low-dimensional rare-earth catalysts, including single-atom [18] and nano-sheet structures, can exhibit enhanced catalytic activity due to strong metal-

[a] RIKEN Center for Emergent Matter Science, 2-1 Hirosawa, Wako, 351-0198, Saitama, Japan. E-mail: kabirsalihu.suraj@riken.jp
[b] Barcelona Supercomputing Center (BSC), 1-3 Plaça Eusebi Güell, 08034, Barcelona, Spain.
[c] Chemistry Department, Faculty of Engineering and Natural Sciences, Istinye University, Sariyer, 34396, Istanbul, Türkiye. E-mail: h.assadi.2008@ieee.org

View Article Online
DOI: 10.1039/D6NR00211K

support interactions and modified $4f$ electronic states. Rare-earth nano-materials supported on oxides have been explored for hydrogen evolution, oxygen evolution, hydrocarbon reforming, and water splitting reactions, where charge transfer and orbital hybridisation play critical roles in determining catalytic efficiency. In particular, the localised nature of $4f$ states and the strong spin-orbit interaction inherent to heavy rare-earth elements provide additional pathways for tuning adsorption strength and electron transfer processes. Despite these developments, the influence of spin-orbit coupling on the $4f$ electronic structure of ultra-thin rare-earth nano-sheets supported on oxide surfaces remains insufficiently understood.

On a more fundamental note, the special theory of relativity dictates that the electric field from the nucleus would appear as a magnetic field in the electron's reference frame. This interaction links the electron's orbital motion with its spin, a phenomenon known as spin-orbit coupling (SOC). The strength of this coupling increases with the fourth power of the atomic number (Z^4), making it particularly strong in heavy rare-earth elements ($Z > 56$). Therefore, due to their larger atomic mass and radii, rare-earth metals exhibit strong spin-orbit coupling, which significantly modifies their electronic structure and can greatly influence catalytic activity. This interaction is also known to cause degeneracy in the f-states of RE elements[19], therefore broadening the spectrum. Such electronic modifications can have a profound impact on catalytic hydrogen processes. Specifically, sharp and deeply localised electronic states can hinder catalysis in two key ways: they increase the energy required for electron transfer from the catalyst to the anti-bonding orbital of the reactant—a critical step in breaking larger hydrogen-containing molecules[17,20]. They raise the likelihood that the density of states (DOS) peak falls outside the optimal energy window, thus stalling the reaction. As a result, catalysts with broader and higher-energy DOS peaks are generally preferred for efficient hydrogen-related catalysis[21]. In this context, lanthanide, with their intrinsic spin-orbit coupling, may offer a distinct advantage over catalysts that lack this feature. Recent advances in rare-earth-based electrocatalysts have demonstrated that the unique partially occupied $4f$ orbitals of RE elements can strongly modulate catalytic activity through electronic redistribution, orbital hybridisation, and spin-dependent interactions. In particular, RE-incorporated nano-materials and oxide-supported catalysts have shown enhanced hydrogen evolution, oxygen evolution, and oxygen reduction performance due to modified electronic structures and improved charge-transfer characteristics. Recent studies have further highlighted the role of SOC and $4f$ orbital modulation in tuning adsorption energetics and catalytic stability in low-dimensional catalytic systems. These findings suggest that relativistic effects and $4f$ electronic restructuring may provide an additional pathway for engineering catalytic activity in rare-earth nano-catalysts[22].

Motivated by these insights, the present study investigates how nano-scale morphology and relativistic spin-orbit coupling collectively impact the electronic structure of and hence the Eu/TiO_2 catalyst interfaces and their potential relevance to hydrogen-related catalytic reactions, including water splitting and hydrocarbon reforming. In particular, we examine how SOC-driven modulation of the Eu $4f$ states may facilitate electron transfer to reactive intermediates through broadening and energetic shifting of the electronic spectrum near the Fermi-level. Previous studies have shown that spin-dependent electronic modulation and strong metal-support interactions are not unique to Eu-based systems, but also occur in other rare-earth catalysts including La- and Gd-containing materials[23,24] used in hydrogen evolution, oxygen evolution, and electrocatalytic reactions. The magnitude of spin-orbit effects is expected to vary across the rare-earth series due to the approximate Z^4 dependence of SOC strength, motivating broader future comparative studies across different rare-earth nano-catalysts and supports.

2 Computational Settings

Both collinear and non-collinear density functional theory (DFT) calculations were performed with VASP[25], using PAW pseudopotentials[26,27] with the following valence configurations: Ti ($3d^3 4s^1$), O ($2s^2 2p^4$), and Eu ($4f^7 6s^2$, with $[\mathrm{Kr}]\,4d^{10}$ treated as core). To enhance the description of systems with strongly correlated d states, an effective on-site Coulomb term U, within the Dudarev formalism[28], was applied to the $3d$ electron. The U value was 4.5 eV, which has been proven to improve TiO_2's band structure description[29–31].

To further examine the role of on-site electronic correlations in the Eu $4f$ states, additional test calculations including a Hubbard correction ($U = 7.0$ eV) on Eu were performed (Supporting Information, Figures S1). The inclusion of U_{Eu} strongly shifts the occupied $4f$ states of the thinner Eu configurations to lower energies and significantly enhances their localisation. Such behaviour is more characteristic of fully oxidised rare-earth compounds with strong oxygen coordination. In contrast, the Eu nano-sheets considered here retain substantial metallic character, with Eu atoms only partially coordinated by oxygen at the interface. Consequently, applying a uniform Hubbard correction to all Eu atoms tends to artificially overlocalise the $4f$ electrons and suppress the metallic and interfacial hybridisation effects central to the present study. By comparison, the thicker Eu configurations, which display more bulk-like metallic behaviour, are considerably less sensitive to U_{Eu}.

The van der Waals dispersion effects were accounted for using the corrections formulated by Grimme and colleagues[32]. The energy and force thresholds were set to be 10^{-5} eV and 0.01 eV/Å. A dense $13 \times 13 \times 1$ k-point mesh generated using the Monkhorst-Pack scheme[33] was used for Brillouin zone sampling to optimize the structure. Higher density meshes ($17\times17\times17$) with tetrahedron smearing were used for DOS calculations. The Lobster code[34] and the Bader Charge Analysis code[35–38] were used to analyse the orbital molecules and charges, respectively.

The models studied here comprised a [001] TiO_2 surface with six symmetric and stoichiometric atomic layers as a support. Metallic Eu was then mounted on the top of this surface. To ensure successful interface simulation pertaining to catalysis, an ample vacuum slab of at least 20 Å was used in all simulations. Four different arrangements (single atom, uni-layered, bi-layered, quadruple layered Eu) of the Eu/TiO_2, both with and without spin-orbit coupling, were examined. The structures presented

View Article Online
DOI: 10.1039/D6NR00211K

here, which were also the most symmetric, were found to be the most stable. It should be mentioned that no symmetry constraints were imposed during the geometry optimisation process to guarantee relaxation to the lowest energy geometry. Furthermore, all atomic internal coordinates and the basal lattice vectors were allowed to relax. Nonetheless, the optimised structures were still symmetric under eight different operations except for the configuration with a single Eu atom, which exhibited symmetry under only two operations. Eu's lattice parameter is 4.578 Å, while for Titania, $a = b = 4.593$ Å, resulting in a highly insignificant basal lattice mismatch of 0.32 % when Eu and TiO_2 were cleaved along the [001] direction. Such a minor lattice mismatch allows the construction of realistic models, as a negligible mismatch between the catalyst and the support ensures ease of epitaxial interface synthesis.

3 Results and Discussion

In the computational design of catalytic nano-metals and nano-alloys with d electrons, the d-band theory is often utilised as a guiding principle. The d-band theory correlates the energy of a metal catalyst's d-band centre of gravity with the adsorption, activation, and dissociation energies of the catalysed molecules[39,40]. Accordingly, modifying the d-band density of states influences the adsorption strength and catalytic activity of a metal surface. The theory is based on interactions between electrons occupying d orbitals of the metal and those of the adsorbate[40]. In particular, the d-band centre serves as a descriptor for d-band electrons; a stronger interaction occurs if the d band centre shifts toward the Fermi-level, and a weaker interaction occurs when it shifts away deeper in the valence band[41].

A factor in the d theory's success is the strong interaction of d electrons with the crystal field, which leads to the removal of d orbital degeneracy, resulting in a relatively broad d-band that is malleable to fine-tuning. However, unlike the d-band theory developed for transition metals, there is no equivalent theoretical framework for $4f$ electrons, as they are highly localised and largely shielded from crystal field effects. Nonetheless, in rare earth elements, due to larger mass, the spin-orbit becomes more significant. The spin-orbit interaction removes the $4f$ degeneracy by coupling each $4f$ electron's spin to the orbital angular momentum, broadening the $4f$ band. Here, we examine the extent to which the SOC broadens the $4f$ and how it affects the bonding of the rare earth catalyst, Eu in this case, to its substrate, TiO_2 in this case. Here, four Eu/TiO_2 interface configurations were investigated, each with and without spin-orbit coupling. The structure shown in Fig. 1A contains one Eu atom supported on a TiO_2 substrate. The density of states of the Eu's $4f$ and topmost oxygen's $2p$ orbitals are shown in Fig. 1B and C for collinear and non-collinear spin alignments, respectively. It can be observed that the interface distance is not affected by spin-orbit coupling as $\delta_1 = 1.944$ in both the collinear and non-collinear cases. Very importantly, the position of the maximum peak denoted by P_{Max} shifts closer to the Fermi-level when spin-orbit coupling is included. For instance, in the single Eu configuration, SOC shifts P_{Max} by approximately 0.70 eV toward the Fermi-level while increasing Δ_{4f} by more than a factor of five, quantitatively demonstrating significant SOC-induced broadening and delocalisation of the Eu $4f$ states. Additionally, the width of the spectrum, which is represented by Δ_{4f} expands as a result of spin-orbit coupling. The DOS is presented in arbitrary units because the different Eu/TiO_2 configurations were calculated using simulation cells of different sizes. In particular, the single-Eu configuration employed a larger supercell to minimise artificial interactions between periodic images of the isolated Eu atom. Consequently, direct comparison of absolute DOS intensities between configurations is not physically meaningful. The analysis therefore focuses primarily on the energetic position, broadening, and overall distribution of the Eu $4f$ states rather than on absolute DOS magnitude.

In Fig. 1D, the structure of a single layer of Eu supported on a TiO_2 is shown. Without spin-orbit coupling, δ_1 is the same as in the single atom case; however, when spin-orbit coupling is included, the distance is slightly lowered. Turning to the density of states (Fig. 1E and F), without spin-orbit coupling, the position of the maximum peak is significantly shifted closer to the Fermi-level and the spread is also increased compared to the single atom case. Here too, P_{Max} shifts closer to the Fermi-level and Δ_{4f} expands as a result of spin-orbit coupling.

Fig. 2A, depicts the bilayer Eu which was supported on a TiO_2. For the collinear case, δ_1 is less than in the previous cases. However, the spin-orbit coupling case shows an improved δ_1 over the collinear case. The distance between the layers, δ_2 was very slightly reduced when spin-orbit coupling was included. Turning to the density of states, we observe that the topmost layers have their P_{Max} values shifted deeper into the valence band in both the collinear (Fig. 2B) and non-collinear (Fig. 2C) cases. Additionally, the Δ_{4f} values reduce in the topmost layers in both cases. Interestingly, P_{Max} shifts closer to the Fermi-level when spin-orbit coupling is included, and Δ_{4f} expands as a result of spin-orbit coupling, as in the previous cases.

In Fig. 2D, the structure of a quadruple layered Eu is shown. Just like in the bilayer case, δ_1 it is reduced as a result of more Eu layers added on top of the oxide support, and the spin-orbit coupling case shows an improved δ_1 over the collinear case. The distances between layers, δ_2 and δ_4 are generally similar while δ_3 is larger and probably closer to a bulk-like structure. Turning to the density of states in Fig. 2E and F, we observe that the P_{Max} values shift away from the Fermi-level the further we go away from the oxide support in both collinear and non-collinear cases. Except for the topmost layer, the Δ_{4f} values decrease with an increase in layer accent in both collinear and non-collinear cases. Interestingly, P_{Max} shifts closer to the Fermi-level when spin-orbit coupling is included, and Δ_{4f} expands as a result of spin-orbit coupling, as in the previous cases.

Deeper and sharper electronic states can harm the catalytic hydrogen process in two ways. First, more energy is required to facilitate electron transfer from the catalyst to the catalysed molecule's anti-bonding state, a step critical for breaking larger hydrogen-bearing molecules[17,20]. Moreover, there is a higher chance that the entire DOS peak will fall outside the optimal energy range, thereby halting the catalytic reaction. These are the reasons why metals with broader DOS and higher-energy peaks are more desirable for catalysis[21].

View Article Online
DOI: 10.1039/D6NR00211K

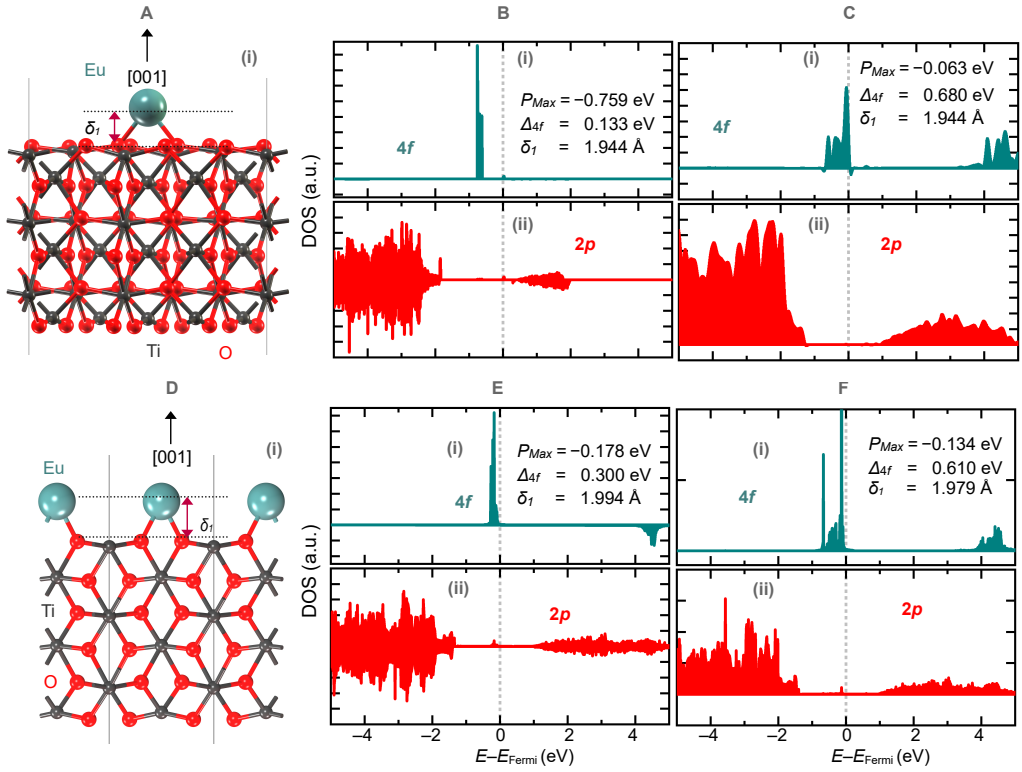

Fig. 1 (A) Optimised structure of the single Eu atom supported on TiO_2. (B) The $4f$ partial density of states for Eu together with that of the inter-facial oxygen $2p$ states without and with (C) spin-orbit coupling for the single atom Eu configuration. Inter-facial oxygens are those atoms directly coordinating Eu. P_{Max} denotes the maximum $4f$ DOS peak, while Δ_{4f} denotes its full width. (D) Optimised structure of the single Eu layer supported on TiO_2. (E) The $4f$ partial density of states for the Eu layer together with that of the inter-facial oxygen's $2p$ states without and with (F) spin-orbit coupling for the one-layered Eu configuration. The corresponding P_{Max} and Δ_{4f} values are indicated directly within each DOS panel for quantitative comparison.

Figures S2–S5 show the Ti d-projected DOS of the TiO_2 substrate for the four Eu configurations: single Eu atom (Fig. S2), one-layer Eu (Fig. S3), two-layer Eu (Fig. S4), and four-layer Eu (Fig. S5), each presented without and with SOC. For all configurations, the Ti d states remain predominantly located away from the Fermi-level, indicating that the intrinsic semiconducting character of TiO_2 is preserved upon Eu adsorption. Inclusion of SOC leads to only minor reshaping and smoothing of the Ti d features, with no substantial SOC-induced states appearing at the Fermi-level. We also observe a weak Ti^{3+}-like contribution near the Fermi-level for low Eu coverage, indicating partial reduction of inter-facial Ti driven by charge transfer from Eu. We also observe a weak Ti^{3+}-like contribution near the Fermi-level for low Eu coverage, indicating partial reduction of interfacial Ti driven by charge transfer from the Eu overlayer. This interfacial charge redistribution is closely connected to the Eu $4f$ electronic structure, particularly the states located near the Fermi-level. Inclusion of SOC broadens the Eu $4f$ spectrum and shifts the principal DOS peaks (P_{Max}) closer to the Fermi-level, thereby increasing the lability of the $4f$ electrons and facilitating charge transfer to the TiO_2 support. As the Eu thickness increases, the Ti d weight near the Fermi-level progressively diminishes, reflecting enhanced electronic screening within the Eu overlayer together with the development of more localised and bulk-like $4f$ states. Consequently, the interfacial Ti gradually recovers a more Ti^{4+}-like electronic character in thicker Eu configurations.

As the Eu thickness increases, this Ti d weight progressively diminishes, reflecting enhanced charge screening within the Eu overlayer and a recovery of bulk-like Ti^{4+} electronic character in the TiO_2 support.

To probe the nature of Eu−O bonding at the interface, we calculated the electronic localisation function (η) and the charge density (ρ) along the Eu−O bond for the four configurations as shown in Fig. S6-S8. Both ρ and η profiles reach their minimum at the middle of the bond for all the configurations, indicating an ionic interaction, especially since the Eu−O bond is relatively short ($\leq$ 2.20 Å). For comparison, the Eu−O bond in EuO, an oxide with more of a covalent nature, is longer at 2.542 Å. For the metallic nano-sheet, the distance between Eu layers varied between 3.481 Å and 3.890 Å, being more prominent than the bulk Eu values of 2.289 Å.

In order to gain further insight into the bonding and anti-bonding characteristics of the Eu electrons in the compounds studied above, we calculated the crystal orbital Hamilton population (COHP) for the four configurations, which we present in Fig. 3. For the single-atom Eu case (Fig. 3a), the interactions between the Eu atom and the topmost oxygen atoms arise predominantly from anti-bonding states located very close to the Fermi-

View Article Online
DOI: 10.1039/D6NR00211K

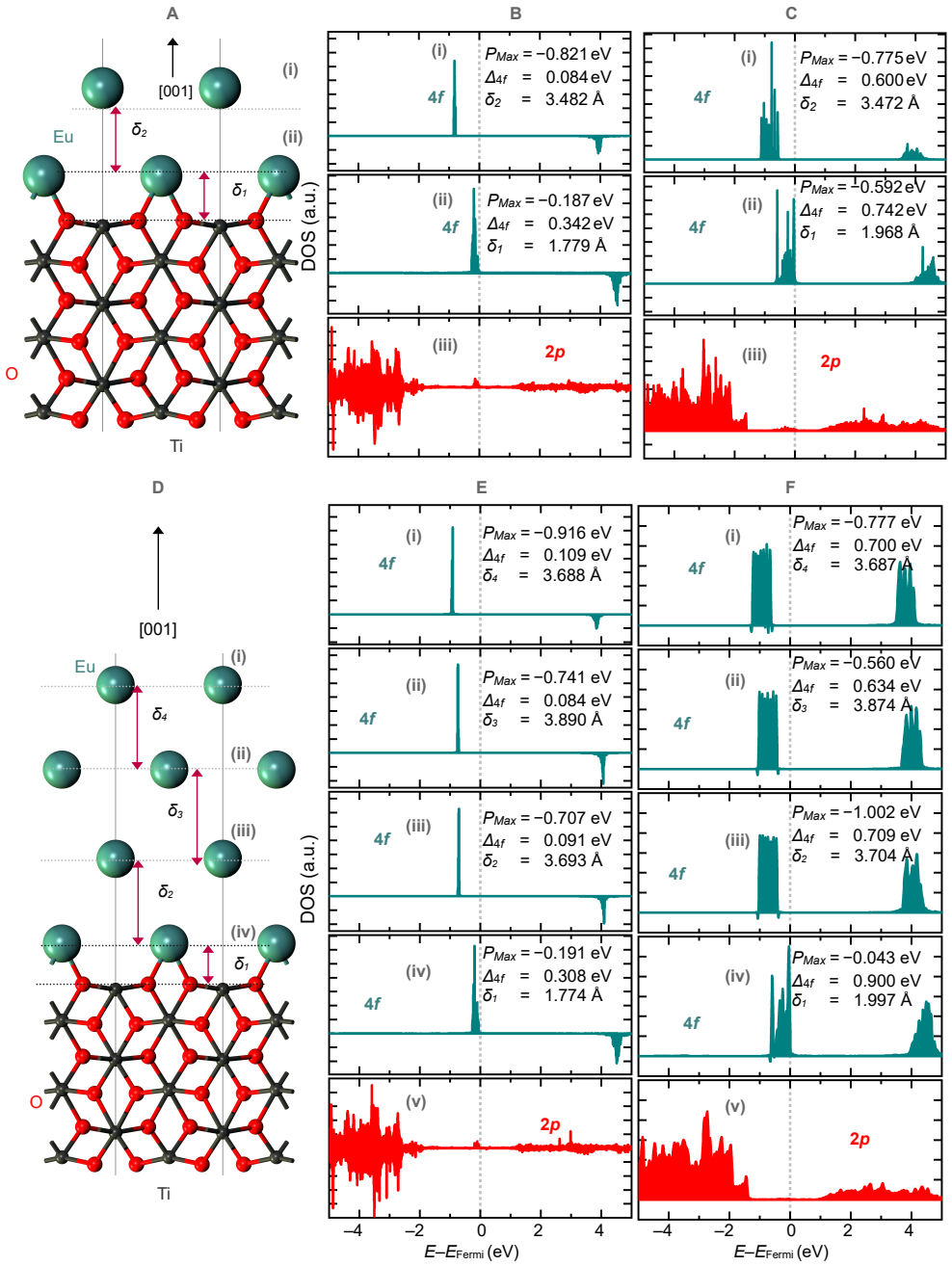

Fig. 2 (A) Optimised structure of the bilayer Eu supported on TiO_2. (B) Layer-resolved $4f$ partial density of states for the Eu layer together with that of the inter-facial oxygen $2p$ states without and with (C) spin-orbit coupling for the two-layered Eu configuration. (D) Optimised structure of the four-layered Eu supported on TiO_2. (E) Layer-resolved $4f$ partial density of states for the Eu layer together with that of the inter-facial oxygen $2p$ states without and with (F) spin-orbit coupling for the four-layered Eu configuration.Corresponding P_{Max} and Δ_{4f} values are indicated directly within each DOS panel for quantitative comparison.

level, indicating a pronounced instability of the Eu−O bond. In the one-layered Eu configuration (Fig. 3b), the Eu−O interactions likewise result from anti-bonding states; however, these peaks appear to be slightly weaker and are shifted further away from the Fermi-level compared to the single-atom case. This shift accounts for the broader Δ_{4f} and the centre of charge (P_{Max}) observed closer to the Fermi-level in the single-layered structure versus the single atom in Figs. 1A-C and 1D-F. In the bilayer and quadruple-layered Eu configurations (Figs. 3c and d), the Eu−O anti-bonding peaks are markedly more intense than the Eu−Eu interlayer anti-bonding interactions. Furthermore, in the bilayer system, the anti-bonding peaks lie closer to the Fermi-level than in the quadruple-layered case, indicating that the Eu−O bond is more unstable in the bilayer than in the quadruple-layered structure.

Finally, we evaluated the formation energies of the four

View Article Online
DOI: 10.1039/D6NR00211K

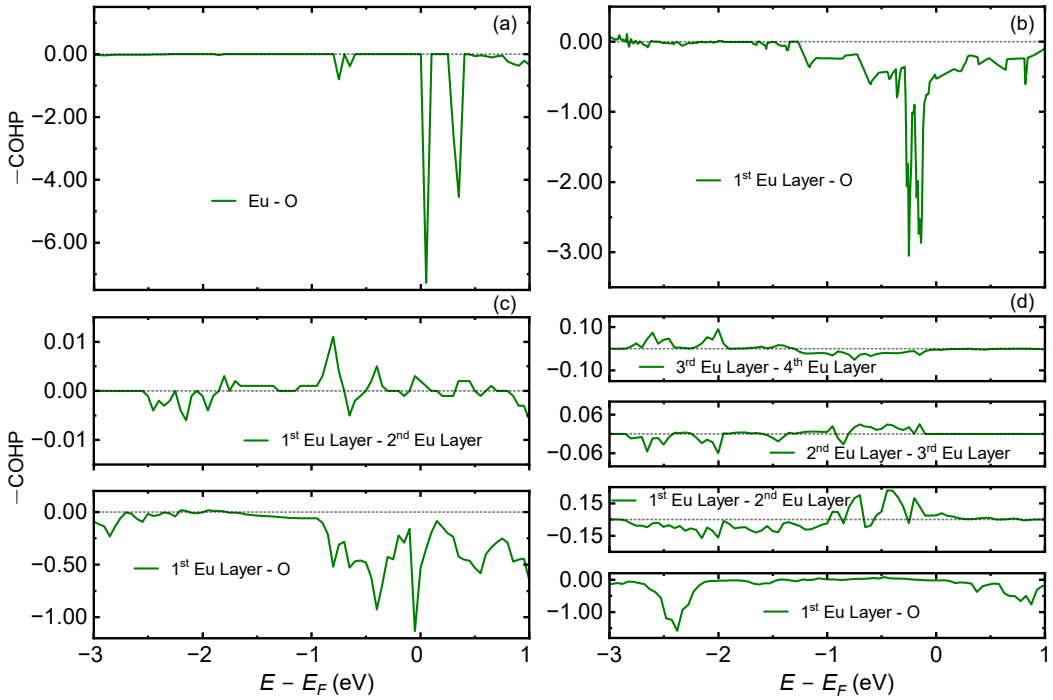

Fig. 3 COHP of the Eu−O and Eu−Eu layers for (a)single Eu atom (b) uni-layer Eu (c) bilayer Eu (d) quadruple Eu configurations

Eu/TiO_2 configurations using

$$\Delta H = E^{\mathrm{DFT}}(\mathrm{Eu/TiO_2}) - E^{\mathrm{DFT}}(\mathrm{Eu}) - E^{\mathrm{DFT}}(\mathrm{TiO_2}). \quad (1)$$

Here, $E^{\mathrm{DFT}}(\mathrm{Eu}) = -10.7718$ which is the total energy contribution stemming from all Eu atoms and $E^{\mathrm{DFT}}(\mathrm{TiO_2}) = -7.3087$, while the corresponding values of $E^{\mathrm{DFT}}(\mathrm{Eu/TiO_2})$ and ΔH for each configuration are listed in Table 1. As anticipated, SOC does not significantly affect the formation energies of any of the four configurations. Notably, the results indicate that stability reduces with increase in the number of Eu layers.

Table 1 The formation energies of the four Eu/TiO_2 configurations (ΔH).

Compound	ΔH without SOC (eV)	ΔH with SOC (eV)
Single Eu atom Eu/TiO_2	−14.1242	−14.1302
One-layer Eu/TiO_2	−4.2615	−4.2666
Two-layer Eu/TiO_2	−2.2167	−1.9198
Four-layer Eu/TiO_2	−1.2999	−1.2870

To provide a more direct connection between the SOC-induced electronic structure modulation and catalytic behaviour, we additionally calculated the adsorption energy of CO on the monolayer Eu/TiO_2 configuration (structure shown in Figure S9) both without and with SOC. The adsorption energy was evaluated using

$$E_{\mathrm{ads}} = E_{\mathrm{DFT}}(\mathrm{Eu/TiO_2 + CO}) - E_{\mathrm{DFT}}(\mathrm{Eu/TiO_2}) - E_{\mathrm{DFT}}(\mathrm{CO}). \quad (2)$$

The calculated adsorption energies are −1.190 eV without SOC and −1.401 eV with SOC, indicating favourable adsorption in both cases. The stronger adsorption obtained with SOC is consistent with the SOC-induced broadening and energetic shifting of the Eu $4f$ states toward the Fermi-level, which enhances electron lability and strengthens the interaction between the catalyst surface and the adsorbed molecule. These results therefore provide direct evidence that SOC-driven electronic modulation influences the interaction of the Eu nano-sheet with catalytically relevant intermediates.

4 Conclusions

Our comprehensive DFT+U investigation demonstrates that, on rutile TiO_2 supports, Eu $4f$ states undergo pronounced SOC-induced splitting and broadening, with principal DOS peaks shifting closer to the Fermi-level. Crucially, the more distal Eu layers develop sharper, deeper $4f$ features that are detrimental to efficient electron transfer in hydrogen-related catalysis. The decreased energy alignment and increased localisation of $4f$ electrons in thicker nano-sheets hinder redox reactivity, favouring configurations with broader, higher-energy DOS peaks. Accordingly, we recommend the synthesis of ultra-thin Eu catalysts—ideally monolayer or sub-monolayer films—to maximise $4f$ contributions near the Fermi-level and optimise catalytic performance for water splitting and hydrocarbon reforming. These findings, highlighting the potential role of spin-orbit coupling in catalysis, align with the historical and emerging consensus in this area. The early understanding of spin's role in catalysis emerged in the 1930s, when paramagnetic molecules, such as O_2 and NO, were observed to induce the interconversion of ortho and para-hydrogen in the gas phase. In contrast, diamagnetic molecules had no such effect[42]. This led to the development of the concept of spin-catalysis, which encompasses phenomena where chemical reactions are promoted by substances that help overcome spin-prohibition or lower activation barriers through spin uncoupling induced by paramagnetic catalysts[43]. The initial theoretical framework proposed by Eyring suggested that paramagnetic cat-

View Article Online
DOI: 10.1039/D6NR00211K

alysts could induce singlet-triplet transitions through inhomogeneous magnetic fields; however, this mechanism was later found to be insufficient to explain the observed effects[44]. Early research also recognised the importance of spin-orbit coupling in transition metal complexes, particularly in biological systems like haemoproteins, where slight modifications of axial ligands could induce spin crossover effects crucial for enzymatic activity[43]. Although the present study focuses primarily on the electronic and catalytic implications of SOC-driven $4f$ modulation, the dynamical and long-term thermal stability of ultra-thin Eu configurations remain important considerations for practical applications. The small lattice mismatch between Eu and TiO_2, together with the interfacial Eu−O interaction, suggests favourable epitaxial stabilisation of the supported nano-sheets. Nevertheless, explicit phonon calculations and finite-temperature investigations of sintering behaviour would provide further insight into the dynamical feasibility and operational stability of these low-dimensional rare-earth catalysts, and therefore constitute an important direction for future work.

More recent understanding has evolved significantly, recognising that spin phenomena are fundamental to catalytic processes, particularly in energy-relevant reactions such as oxygen reduction and evolution[45,46]. Three key types of spin dependence in catalysis have been identified: quantum spin exchange interactions (QSEI); direct spin-spin interactions (DSSI); and strong spin-orbit couplings, particularly in chiral structures[47]. These spin interactions are now known to be entangled; when DSSI or spin-orbit coupling potentials stabilise a magnetic structure, repulsions among spin-oriented electrons decrease due to internal QSEI. This new understanding has particularly impacted the development of electrocatalysts for green hydrogen production, where spin-magnetic potentials enhance performance by $10 \sim 50\%$[48]. Here, we demonstrate that spin-orbit interaction can enhance catalyst performance by modulating electron lability and metal-support binding. By broadening the electron lability window and altering the catalyst's electronic structure, the predicted spin-orbit effect is speculated to have a greater influence than either DSSI or QSEI.

Author contributions

Kabir S. Suraj: Software, Investigation, Writing of original draft, J. Julio Gutiérrez Moreno: Software, Conceptualization, and M. Hussein N. Assadi: Software, Conceptualization, Investigation.

Conflicts of interest

The authors declare that they have no known competing financial interests or personal relationships that could have appeared to influence the work reported in this paper.

Data availability

The data that support the findings of this study are available from the corresponding author upon reasonable request.

Acknowledgments

The computing resources were provided by the HOKUSAI system at RIKEN. This research was supported by funding from the Japan Science and Technology Agency (JST) and the Spanish State Research Agency (project no. PCI2023-143426 funded by MCIN/AEI/10.13039/501100011033 and the European Union) as participants of the EIG CONCERT-JAPAN program under the project entitled 2023-MLALH. J.J.G.M acknowledges his AI4S fellowship within the "Generación D" initiative by Red.es, Ministerio para la Transformación Digital y de la Función Pública, for talent attraction (C005/24-ED CV1), funded by NextGenerationEU through PRTR.

Notes and references

1 W. Zhan, Y. Guo, X. Gong, Y. Guo, Y. Wang and G. Lu, *Chin. J. Catal.*, 2014, **35**, 1238–1250.
2 Z.-H. Pan, Z.-Z. Weng, X.-J. Kong, L.-S. Long and L.-S. Zheng, *Coord. Chem. Rev.*, 2022, **457**, 214419.
3 H. Liu, Y. Jiang, K. Jiang, Z. He, Z. Zhong, C. Gu and Y. Du, *Adv. Funct. Mater.*, 2025, **36**, e25512.
4 H. B. Kagan, *Chem. Rev.*, 2002, **102**, 1805–1806.
5 H. Wang, X. Pan, Y. Wang, B. K. Y. Ng and S. C. E. Tsang, *Appl. Catal. A*, 2025, **691**, 120055.
6 A. Gaur, J. Sharma, E. Enkhbayar, M. S. Cho, J. H. Ryu and H. Han, *EcoMat*, 2024, **6**, e12484.
7 W. Gao, D. Wen, J. Ho and Y. Qu, *Mater. Today Chem.*, 2019, **12**, 266–281.
8 Y. T. Shah and T. H. G. and, *Catal. Rev.*, 2014, **56**, 476–536.
9 T. Wu, M. Sun, B. Huang and Y. Du, in *Rare-earth Nanomaterials for PEC Energy Conversion*, John Wiley & Sons, Ltd, 2022, ch. 16, pp. 399–410.
10 P. Singh, S. Kachhap, P. Singh and S. Singh, *Coord. Chem. Rev.*, 2022, **472**, 214795.
11 K. M. Katubi, M. U. Nisa, S. Manzoor, Z. Ahmad, A. G. Abid, M. Abdullah, M. S. Al-Buriahi and M. N. Ashiq, *Appl. Phys. A*, 2022, **128**, 882.
12 E. Doustkhah, M. Hasani, Y. Ide and M. H. N. Assadi, *ACS Appl. Nano Mater.*, 2019, **3**, 22–43.
13 S. Ren, Q. Yu, X. Yu, P. Rong, L. Jiang and J. Jiang, *Sci. China Mater*, 2020, **63**, 903–920.
14 M. D. Yadav, H. M. Joshi, S. V. Sawant, K. Dasgupta, A. W. Patwardhan and J. B. Joshi, *Chem. Eng. Sci.*, 2023, **272**, 118586.
15 E. Doustkhah, A. Kotb, S. Tafazoli, T. Balkan, S. Kaya, D. A. Hanaor and M. H. N. Assadi, *ACS Mater. Au*, 2023, **3**, 231–241.
16 E. Doustkhah, R. Hassandoost, A. Khataee, R. Luque and M. H. N. Assadi, *Chem. Soc. Rev.*, 2021, **50**, 2927–2953.
17 E. Doustkhah, N. Tsunoji, M. H. N. Assadi and Y. Ide, *Adv. Mater. Interfaces*, 2023, **10**, 2202368.
18 M. B. Gawande, K. Ariga and Y. Yamauchi, *Small*, 2021, **17**, 2101584.
19 I. Sk, J. Chatterjee, A. Taraphder and N. Pakhira, *EPJ B.*, 2025, **98**, 1–7.
20 J. H. Sinfelt, *Acc. Chem. Res.*, 1977, **10**, 15–20.
21 H. Wu, J. Zhang, Q. Lu, Y. Li, R. Jiang, Y. Liu, X. Zheng, N. Zhao, J. Li, Y. Deng *et al.*, *ACS Appl. Mater. Interfaces*, 2023, **15**, 38423–38432.

View Article Online
DOI: 10.1039/D6NR00211K

22 X. Wang, Y. Tang, J.-M. Lee and G. Fu, *Chem Catal.*, 2022, **2**, 967–1008.
23 M. He, P. Wang, J. Yao, Y. Li, S. Meng and Z. Li, *J. Rare Earths*, 2025, **43**, 1091–1099.
24 E. E. Gordon, X. Cheng, J. Kim, S.-W. Cheong, S. Deng and M.-H. Whangbo, *Inorg. chem.*, 2018, **57**, 9260–9265.
25 G. Kresse and J. Furthmüller, *Comput. Mater. Sci.*, 1996, **6**, 15–50.
26 P. E. Blochl *et al.*, *Phys. rev. B*, 1994, **50**, 17953–17979.
27 G. Kresse and D. Joubert, *Physical review b*, 1999, **59**, 1758.
28 S. L. Dudarev, G. A. Botton, S. Y. Savrasov, C. J. Humphreys and A. P. Sutton, *Phys. Rev. B*, 1998, **57**, 1505–1509.
29 S. E. Shirsath, M. H. N. Assadi, J. Zhang, N. Kumar, A. S. Gaikwad, J. Yang, H. E. Maynard-Casely, Y. Y. Tay, J. Du, H. Wang *et al.*, *ACS nano*, 2022, **16**, 15413–15424.
30 J. J. Gutiérrez Moreno and M. Nolan, *ACS Appl. Mater. Interfaces*, 2017, **9**, 38089–38100.
31 J. J. G. Moreno, M. Fronzi, P. Lovera, A. O'Riordan, M. J. Ford, W. Li and M. Nolan, *Phys. Chem. Chem. Phys.*, 2019, **21**, 25344–25361.
32 S. Grimme, J. Antony, S. Ehrlich and H. Krieg, *J. Chem. Phys.*, 2010, **132**, 154104.
33 H. J. Monkhorst and J. D. Pack, *Phys. Rev. B*, 1976, **13**, 5188–5192.
34 S. Maintz, V. L. Deringer, A. L. Tchougréeff and R. Dronskowski, *J. Comput. Chem.*, 2016, **37**, 1030–1035.
35 M. Yu and D. R. Trinkle, *J. Chem. Phys.*, 2011, **134**, 064111.
36 G. Henkelman, A. Arnaldsson and H. Jónsson, *Comput. Mater. Sci.*, 2006, **36**, 354–360.
37 E. Sanville, S. D. Kenny, R. Smith and G. Henkelman, *J. Comput. Chem.*, 2007, **28**, 899–908.
38 W. Tang, E. Sanville and G. Henkelman, *J. Phys.: Condens. Matter*, 2009, **21**, 084204.
39 M. T. Gorzkowski and A. Lewera, *J. Phys. Chem. C*, 2015, **119**, 18389–18395.
40 X. Wang, G. Zhang, L. Yang, E. Sharman and J. Jiang, *Wiley Interdiscip. Rev. Comput. Mol. Sci.*, 2018, **8**, e1369.
41 S. Jiao, X. Fu and H. Huang, *Adv. Funct. Mater.*, 2022, **32**, 2107651.
42 B. F. Minaev and H. Aagren, *J. Phys. Chem.*, 1995, **99**, 8936–8940.
43 B. F. Minaev and H. Ågren, *Int. J. Quantum Chem.*, 1996, **57**, 519–532.
44 B. Minaev, *Theor. Exp. Chem.*, 1996, **32**, 1–12.
45 J. Gracia, *Phys. Chem. Chem. Phys.*, 2017, **19**, 20451–20456.
46 S. Sun, Y. Zhang, X. Shi, W. Sun, C. Felser, W. Li and G. Li, *Adv. Mater.*, 2024, **36**, 2312524.
47 C. Biz, M. Fianchini and J. Gracia, *ACS Catal.*, 2021, **11**, 14249–14261.
48 J. Gracia, C. Biz and M. Fianchini, *Phys. Chem. Chem. Phys.*, 2024, **26**, 22620–22639.

View Article Online
DOI: 10.1039/D6NR00211K

The data that support the findings of this study are available from the corresponding author upon reasonable request